Hck contributes to bone homeostasis by controlling the recruitment of osteoclast precursors

Christel Vérollet,*,†,‡ Anne Gallois,§ Romain Dacquin,‖,¶ Claire Lastrucci,*,†,‡
Subramanya N. M. Pandruvada,‖,¶ Nathalie Ortega,*,†,‡ Renaud Poincloux,*,†,‡
Annie Behar,*,†,‡ Céline Cougoule,*,†,‡ Clifford Lowell,# Talal Al Saati,**
Pierre Jurdic,‖,¶ and Isabelle Maridonneau-Parini*,†,‡,1

*Centre National de la Recherche Scientifique (CNRS), Unité Mixte de Recherche (UMR) 5089, Institut de Pharmacologie et de Biologie Structurale (IPBS), Toulouse, France; †Université de Toulouse, Toulouse, France; ‡Université Paul Sabatier (UPS), Toulouse, France; §New York University Langone Medical Center Cancer Institute, New York, New York, USA; ‖Institut de Génomique Fonctionnelle de Lyon, UMR 5242, Université de Lyon 1, Lyon, France; ¶CNRS, Ecole Normale Supérieure de Lyon, Lyon, France; #Department of Laboratory Medicine, University of California, San Francisco, California, USA; and **Unité Institut National de la Santé et de la Recherche Médicale (INSERM)/UPS, US006/Centre Régional d'Exploration Fonctionnelle et Ressources Expérimentales (CREFRE), Service d'Histopathologie, Centre Hospitalier Universitaire (CHU) Purpan, Toulouse, France

ABSTRACT   In osteoclasts, Src controls podosome organization and bone degradation, which leads to an osteopetrotic phenotype in $src^{-/-}$ mice. Since this phenotype was even more severe in $src^{-/-}hck^{-/-}$ mice, we examined the individual contribution of Hck in bone homeostasis. Compared to *wt* mice, $hck^{-/-}$ mice exhibited an osteopetrotic phenotype characterized by an increased density of trabecular bone and decreased bone degradation, although osteoclastogenesis was not impaired. Podosome organization and matrix degradation were found to be defective in $hck^{-/-}$ osteoclast precursors (preosteoclast) but were normal in mature $hck^{-/-}$ osteoclasts, probably through compensation by Src, which was specifically overexpressed in mature osteoclasts. As a consequence of podosome defects, the 3-dimensional migration of $hck^{-/-}$ preosteoclasts was strongly affected *in vitro*. *In vivo*, this translated by altered bone homing of preosteoclasts in $hck^{-/-}$ mice: in metatarsals of 1-wk-old mice, when bone formation strongly depends on the recruitment of these cells, reduced numbers of osteoclasts and abnormal developing trabecular bone were observed. This phenotype was still detectable in adults. In summmary, Hck is one of the very few effectors of preosteoclast recruitment described to date and thereby plays a critical role in bone remodel-

ing.—Vérollet, C., Gallois, A., Dacquin, R., Lastrucci, C., Pandruvada, S. M. N., Ortega, N., Poincloux, R., Behar, A., Cougoule, C., Lowell, C., Al Saati, T., Jurdic, P., Maridonneau-Parini, I. Hck contributes to bone homeostasis by controlling the recruitment of osteoclast precursors. *FASEB J.* 27, 3608–3618 (2013). www.fasebj.org

BONE IS RENEWED CONTINUOUSLY by a process known as bone remodeling. Bone remodeling is accomplished by 3 cell types: osteocytes, osteoblasts, and osteoclasts (OCs). Osteocytes are the mechanical sensors of bone that regulate osteoclast formation. Osteoblasts synthetize the matrix and promote its mineralization, while OCs are responsible for degradation of bones during bone development, homeostasis, and repair. The formation and degradation of bone are tightly balanced in both time and space. A dysregulation of this tight balance between bone formation and bone degradation may result either in loss of bone mass, such as in osteoporosis, or in contrast, in a progressive increase in bone mass, such as in osteopetrosis. Degrading OCs are large multinucleated giant cells formed by the differentiation and fusion of mononuclear monocyte lineage precursors after stimulation by receptor activator of nuclear factor κ-B ligand (RANKL) and macrophage colony-stimulationg factor (M-CSF) (1–3). They are characterized by high levels of cathepsin K and tartrate resistant acidic phosphatase (TRAP) activities, which

---

Abbreviations: 3D, 3-dimensional; BV/TV, bone volume/tissue volume; cortical th., cortical thickness; DPD, deoxypyridinoline; Hck, hematopoietic cell kinase; HRP, horseradish peroxidase; LSM, lymphocyte separation medium; M-CSF, macrophage colony-stimulating factor; MMP, matrix metalloprotease; pre-OC, osteoclast precursor; OC, osteoclast; PBS, phosphate-buffered saline; PINP, procollagen type I N-terminal propeptide; RANKL, receptor activator of nuclear factor κ-B ligand; SFK, Src family kinase; TRAP, tartrate resistant acidic phosphatase; Tb.N, trabecular number; Tb. Sep, trabecular separation; v-ATPase, vacuolar proton pump; WT, wild type

can be used as markers of OC differentiation. OC precursors (pre-OCs) are found in hematopoietic tissues and gain access, through blood circulation, to the bone, where they find the suitable stromal environment for their terminal differentiation into OCs (4, 5). OCs are involved in bone degradation by 3 main processes: adhesion to the bone surface *via* a structure called the sealing zone; acidification of the subosteoclastic bone-resorbing compartment through vacuolar proton pump (v-ATPase); and secretion of hydrolytic enzymes (mainly cathepsin K and metalloproteases). The sealing zone mediates attachment to the bone surface and bone degradation. It is composed of an actin ring that is the equivalent of podosome belts observed in glass adherent osteoclasts (6–8). Podosomes are highly dynamic F-actin-rich adhesion structures with proteolytic properties, surrounded by numerous actin-linked proteins, such as vinculin (9). They are found in OCs and a few other cell types of the monocyte lineage, such as macrophages and dendritic cells. In OCs, podosomes are mostly organized as clusters, rings, and, finally, as belts, when OCs are mature (10).

The nonreceptor tyrosine kinase Src has been identified as one of the first proteins essential for normal OC function (11, 12). $src^{-/-}$ mice are severely osteopretrotic due to dysfunctional OCs (11, 13–15), which display abnormal podosome organization and are unable to form sealing zones, which thus prevents them from resorbing bone (12, 16). Among the other Src family kinases (SFKs) expressed in OCs (Lyn, Yes, Fgr, and Hck), only the expression of hematopoietic cell kinase (Hck) is up-regulated in $src^{-/-}$ OCs (17). Notably, $src^{-/-}hck^{-/-}$ double mutants develop a more severe form of osteopetrosis than $src^{-/-}$ mice (14, 15, 17, 18). In contrast, $fgr^{-/-}src^{-/-}$ mice do not develop more severe osteopetrosis than $src^{-/-}$ mice, which indicates that Fgr does not compensate for Src deletion. These data suggest that Hck, which is expressed only in myeloid-derived cells, could partially compensate for Src deficiency in OCs (19, 20). Of interest, in OCs, both Hck and Src are present at podosome belts (16, 21, 22). In macrophages, Hck controls podosome stability and organization as rosettes (23, 24), structures involved in the migration process in 3-dimensional (3D) environments (23–27). The role of Hck in OCs has not been explored.

In the present study, we used a loss-of-function approach to study the specific role of Hck in bone homeostasis. We found that $hck^{-/-}$ mice display an osteopetrotic phenotype characterized by a high trabecular bone mass. The absence of Hck did not affect the formation of OCs *in vitro*, and the organization of podosomes and the bone-resorption activity in these cells were normal. However, in $hck^{-/-}$ pre-OCs, the formation of podosomes and their organization as rosettes were strongly affected. As a consequence, *in vitro* migration was defective. In 1-wk-old $hck^{-/-}$ mice, a reduced number of TRAP-positive cells were recruited on bone, which exhibit defective trabecular bone remodeling. In $hck^{-/-}$ adult mice, the number of OCs was still reduced. We propose that an impaired recruitment of pre-OCs to trabecular bone could explain osteopetrosis in $hck^{-/-}$ mice.

MATERIALS AND METHODS

Kits and reagents

Lymphocyte separation medium (LSM) was purchased from Eurobio (Courtaboeuf, France). α-MEM and fetal calf serum were from Invitrogen (Carlsbad, CA, USA) and Bio West (Logan, UT, USA), respectively. Leukocyte acid phosphatase kit for TRAP staining and DAPI were purchased from Sigma (Lyon, France). Rabbit polyclonal anti-Hck (sc-72), anti-Src, anti-Lyn, and anti-cathepsin K antibodies were purchased from Santa Cruz Biotechnologies (TEBU-Bio, Le Perray-en-Yvelines, France). Monoclonal anti-actin and mouse anti-vinculin (clone hVin-1) were purchased from Sigma. Secondary horseradish peroxidase (HRP)-conjugated antibodies were from Bio-Rad (Hercules, CA, USA), and Alexa Texas Red/488/633-coupled phalloidins were obtained from Molecular Probes (Invitrogen). Matrigel (10–12 mg/ml) was purchased from BD Biosciences (San Jose, CA, USA).

Mice

$hck^{-/-}$ mice, backcrossed onto the C57Bl6/J background, were previously characterized (28). All experiments were performed according to animal protocols approved by the Animal Care and Use committee of the Institut de Pharmacologie et de Biologie Structurale.

Bone histomorphometric analysis

Bone (femurs and tibia) were fixed in PBS plus 4% paraformaldehyde overnight at 4°C and then washed and stored in 70% ethanol. Three-dimensional microarchitecture of the distal femur and the tibia from 3-mo-old wild-type (*wt*) and $hck^{-/-}$ female littermate mice was evaluated using a high-resolution SkyScan1076 microtomographic imaging system (SkyScan, Kontich, Belgium). Images were acquired at 48 KeV, 200 mA with a 0.5-mm aluminum filter. Three-dimensional reconstructions (8.8-mm cubic resolution) were generated using NRecon software (SkyScan) as described previously (29). High-resolution images (2.5 μm) were obtained using the Nanotom device from Phenix X-ray (GE Measurement and Control Solutions; GE, Dresden, Germany). Measurements of bone cell parameters and architecture parameters were performed with the OsteoMeasure Analysis System (OsteoMetrics, Decatur, GA, USA) using a 3CCD color video DXC-390 camera (Sony, Tokyo, Japan) coupled to a Leica microscope (Leica Microsystems, Wetzlar, Germany), according to standard procedure. Animal groups were composed of 10 mice.

Bone marker analysis

Serum and urine from 3-mo-old *wt* and $hck^{-/-}$ littermate mice were collected. Bone-related degradation products from type 1 collagen, deoxypyridinoline (DPD) cross-links, and creatine were measured in evening urine using the Pyrilinks-D immunoassay and creatine kit (Quidel Corp., San Diego, CA, USA), according to the manufacturer's protocols. Bone formation residues were measured by using the procollagen type I N-terminal propeptide (PINP) rat and mouse ELISA kit from Immuno Diagnostic System (Paris, France). Animal groups were composed of a minimum of 8 mice.

Histological analysis

Metatarsals were dissected from 1-wk-old $hck^{-/-}$ mutant animals and *wt* littermate controls and were fixed in 4% paraformaldehyde at 4°C overnight. The tissues were then washed in phosphate-buffered saline (PBS) and decalcified

in 0.5 M EDTA (pH 7.4), as described previously (30). Paraffin sections (5 μm) were stained with Safranin O and Fast Green (Sigma). For TRAP staining, sections were deparaffinized and rehydrated and stained using a leukocyte acid phosphatase kit and Fast Red Violet as a substrate (Sigma) at 37°C for 1 h. The sections were then washed in distilled water and counterstained with hematoxylin.

Femurs and tibia from adult *wt* and *hck*$^{-/-}$ littermate mice were fixed in 10% buffered formalin solution (Sigma), decalcified in EDTA, and embedded in paraffin. Longitudinal serial sections of the median portion of whole bone were stained for TRAP (Sigma) according to the manufacturer's protocols and were counterstained with hematoxylin. Stained slides were digitized using Panoramic 250 Flash digital microscope (P250 Flash; 3DHisTech, Budapest, Hungary). Whole slides were scanned in brightfield scan mode with a ×40/NA 0.8 Zeiss Plan-Apochromat dry objective, and images were acquired with a 2-megapixel 3CCD color camera (CIS Cam VCC-F52U25CL; CIS Americas Inc., Gilbert, AZ, USA). This objective and camera combination yield a 0.22-μm/pixel resolution in fluorescence scan mode, which corresponds, in conventional microscopy, to ×56.09 magnification at the highest optical resolution. Panoramic Viewer (RTM 1.15.0.53) was used for viewing, analysis, and quantification of the digital slides. TRAP-positive cells were quantified. Animal groups were composed of a minimum of six mice. Mononucleated and multinucleated TRAP-positive cells were counted on ≥ 6 serial sections chosen among the most median part of 4 different metatarsals for each genotype.

OC differentiation

Bone marrow mononuclear cells from 8-wk-old *wt* and *hck*$^{-/-}$ mice were cultured for 5 to 6 d at a cell density of 500 cells/mm^2 in the presence of α-MEM containing 10% (v/v) fetal calf serum, M-CSF (20 ng/ml), and RANKL (30 ng/ml) on glass or, when mentioned, on BioCoat ostologic bone slices (Becton Dickinson, Franklin Lakes, NJ, USA). We have previously shown that pre-OCs, mononucleated cells, are obtained after 3 d of culture of mouse precursors, whereas mature OCs which are large multinucleated cells with a high number of nuclei (are considered OC cells with ≥2 nuclei), are obtained at d 5 and 6 of differentiation (31).

Cell lysis and immunoblotting

Cells were lysed, and total proteins were separated through 7.5% SDS-polyacrylamide gel electrophoresis, transferred, and immunoblotted as described previously (32). For cathepsin K, 10 μg (cell lysates) and 1 μg protein samples (serum starved cell-conditioned medium collected overnight) were subjected to 10% SDS-PAGE and blot-transferred on a nitrocellulose membrane. Blocking was performed with 5% nonfat dry milk in TBS-T (50 mM Tris, pH 7.2; 150 mM NaCl; and 0.1% Tween 20) for 1 h, followed by anti-cathepsin K (Santa Cruz Biotechnology) overnight at 4°C. The blots were then incubated for 1 h with secondary antibody conjugated to HRP and developed using the electrochemiluminescence (ECL) system. Expression of actin using anti-β-actin antibody (Sigma) was used to normalize loading variations with respect to cell lysates only. For Hck, Src, and Lyn, immunoblotting was performed as described previously (33).

Gelatin zymography

OC cell-conditioned medium was analyzed for matrix metalloprotease 9 (MMP9) activity by gelatin substrate gel electrophoresis (34). Samples of serum-starved cell culture medium
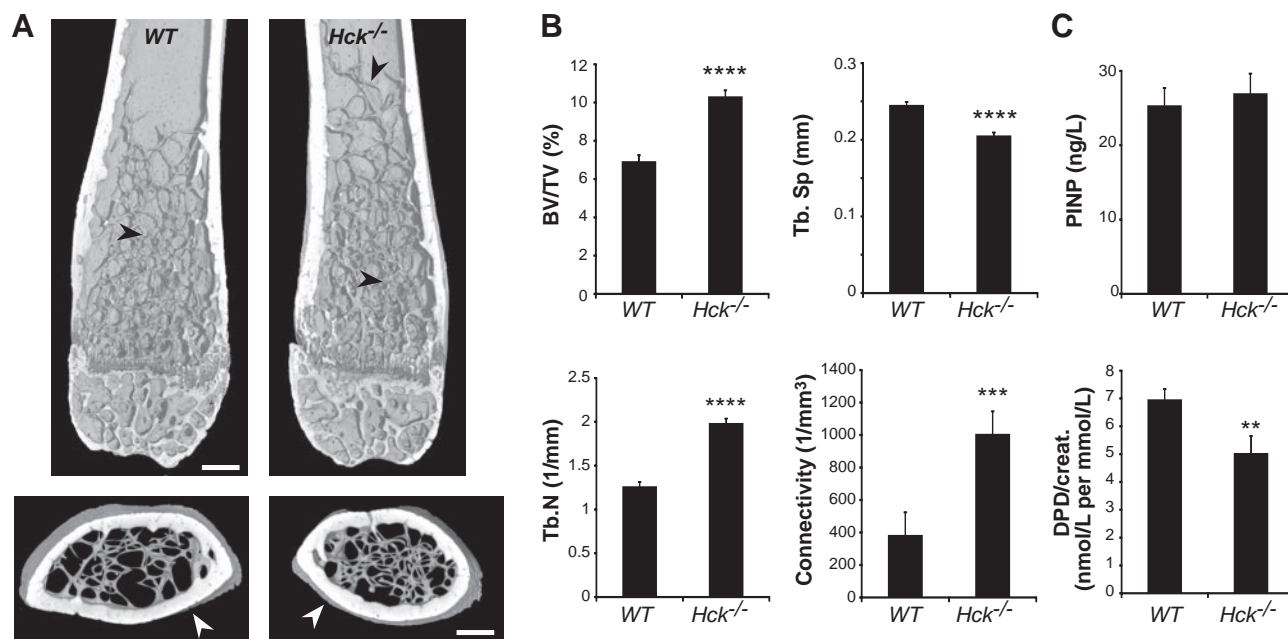
Figure 1. *Hck*$^{-/-}$ mice have a high trabecular bone mass, due to bone degradation defects. *A*) High-resolution micro-computed tomography (micro-CT) images of femurs of 3-mo-old *wt* and Hck-deficient (*hck*$^{-/-}$) mice. White arrowheads show cortical bone; black arrowheads show trabecular bone. Trabecular bone is more dense in *hck*$^{-/-}$ mice. Scale bars = 500 μm. *B*) Bone microarchitecture parameters are modified in *hck*$^{-/-}$ mice: bone volume/tissue volume (BV/TV), trabecular number (Tb. N), trabecular separation (Tb. Sep), and connectivity. Data were obtained from 10 mice/phenotype. Error bars = SEM. *C*) Biochemical markers of bone turnover. PINP and DPD levels were measured in serum and urine samples, respectively, from 3-mo-old control and *hck*$^{-/-}$ mice. DPD level is decreased in *hck*$^{-/-}$ mice. Data were obtained from 10 mice/phenotype. Error bars = SEM.

containing 1 µg protein were electrophoresed in the absence of reducing agents to a 10% SDS-PAGE containing 0.1% gelatin. After electrophoresis, the gels were washed in renaturing buffer (50 mM Tris-HCl, pH 7.5, and 2.5% Triton X-100) for 30 min at room temperature and then incubated overnight at 37°C in the developing buffer (50 mM Tris-HCl, 200 mM NaCl, 5 mM $CaCl_2$, and 0.02% w/v Brij 35). The gels were stained with a solution containing 0.1% Coomassie Brilliant Blue R-250. Formation of clear zone against the blue background on the polyacrylamide gels indicated the gelatinolytic activity.

Resorption assays

To assess resorption activity, bone marrow mononuclear cells were cultured on bovine cortical bone slices for 10 d in the presence of α-MEM containing 10% (v/v) fetal calf serum, supplemented with M-CSF (20 ng/ml) and RANKL (30 ng/ml). Following complete cell removal by immersion in water and scraping, bone slices were stained with toluidine blue to detect resorption pits under a light microscope (Leica DMIRB, Leica Microsystems; ref. 35).

Microscopy and live analysis of cell fusion and migration

Cells in the course of differentiation were fixed and stained as described previously (33) and visualized using a Leica DM-RB fluorescence microscope as described previously (23, 36). Quantification of OC surface, number, and fusion index (total number of nuclei in OCs divided by total number of nuclei × 100) were assessed using Image J software (U.S. National Institutes of Health, Bethesda, MD, USA). All images were prepared with Adobe Photoshop software (Adobe Systems, San Jose, CA, USA). For measurement of migration in Matrigel, pictures of cells were taken automatically with an ×10 objective at constant intervals using the monitorized stage of an inverted microscope (Leica DMIRB); cells were counted using ImageJ as described previously (37). For live analysis of pre-OC fusion, bone marrow mononuclear cells were plated for differentiation into OCs in observation chambers (Lab-tek; Nalge Nunc International, Naperville, IL, USA), and transduced with mCherry-Lifeact lentiviral vector (10^6 effective viral particles for 10^6 cells) at d 2 of culture as described previously (38). They were imaged during the night between d 4 and 5 (1 image every 2 min) with a Leica DMIRB microscope. Movies were prepared with ImageJ software.

Migration assays *in vitro*

Migration assays and quantification were performed as described previously (37) except that after 48 h of migration, living cells were stained with SYTO16 (Invitrogen) to discriminate mononucleated cells and multinulceated OCs.

Statistical analysis

Statistical differences were analyzed with Student's *t* test, and error bars represent sem. Values of $P \leq 0.01$ were considered significant.

RESULTS

$hck^{-/-}$ mice are osteopetrotic

As $src^{-/-}hck^{-/-}$ double-knockout mice develop more severe osteopetrosis than the $src^{-/-}$ animals (17), we investigated whether bone phenotype was affected in $hck^{-/-}$ single mutant. First, we performed bone histomorphometric analysis on femurs of 3-mo-old mice to evaluate the effect of Hck deficiency on bone. As shown in **Fig. 1***A*, $hck^{-/-}$ mice were osteopetrotic with numerous trabeculae compared with those of their *wt* littermates, whereas cortical bone parameters were unchanged (Supplemental Fig. S1). Quantification of trabecular bone parameters revealed a significant increase of the bone mass in Hck-deficient mice compared to *wt* (Fig. 1*A*, *B*), an enhanced trabecular number and connectivity density, and a decrease in trabecular separation (Fig. 1*B*). Then, we tested the parameters of bone formation and resorption *in vivo*. Urine and blood samples were collected to analyze the level of bone turnover markers. As expected for cells that do not express Hck (39), the function of osteoblasts was not affected in $hck^{-/-}$ mice since similar levels of PINP, a marker of bone formation, were found in the serum of *wt* and $hck^{-/-}$ mice (Fig. 1*C*). In contrast, we observed reduced bone-resorption activity in $hck^{-/-}$ mice, as levels of the urine DPD cross links, a bone-related degradation product, were significantly decreased (Fig. 1*C*).
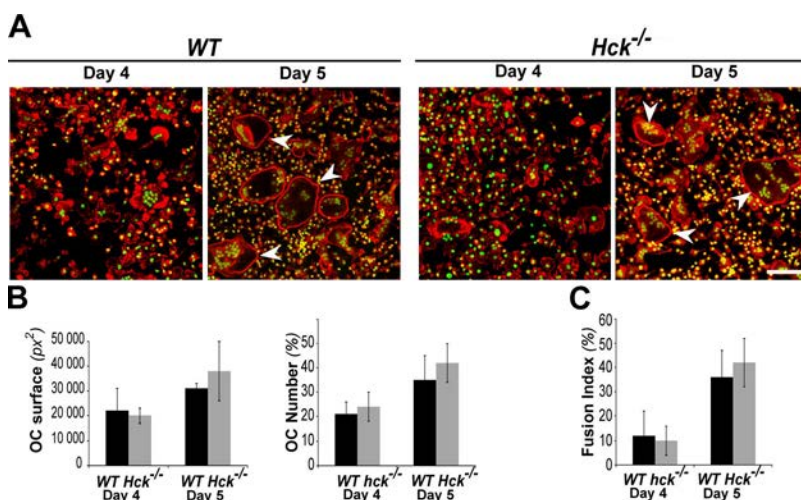
Figure 2. Formation of $hck^{-/-}$ mature OCs *in vitro* is normal. *A*) Bone marrow mononuclear cells from *wt* and $hck^{-/-}$ mice were seeded on glass coverslips in the presence of M-CSF and RANKL to promote OC differentiation. Cells were fixed at the indicated times and stained with Texas red-coupled phalloidin (F-actin, red) and DAPI (nuclei in green). Merged images representative of 7 experiments are shown. White arrowheads show large and mature OCs with their typical F-actin belts. Scale bar = 100 µm. *B*, *C*) Automatic quantification (Image J) of OC surface, number (*B*), and fusion index (*C*) at d 4 and 5 of differentiation. Data were obtained from 5 independent experiments. Error bars = sd.

These results indicate that $hck^{-/-}$ mice display an osteopetrotic phenotype characterized by a high trabecular bone mass, and this is probably caused by a decreased bone degradation activity.

Absence of Hck does not affect OC formation

To investigate whether the osteopetrotic phenotype of $hck^{-/-}$ mice could be the result of impaired osteoclastogenesis, we examined the *in vitro* differentiation of bone marrow mononuclear cells isolated from *wt* and $hck^{-/-}$ mice. Osteoclastogenesis was triggered by the combination of two cytokines, M-CSF and RANKL, and the multinucleation process was measured as described previously (33). At d 4, 5 (**Fig. 2A**), and 6 (data not shown) of differentiation, the number of OCs, their size, and the fusion index were comparable in *wt* and $hck^{-/-}$ cells (Fig. 2). In addition, no difference was

observed in the viability of *wt* and $hck^{-/-}$ OCs (data not shown). Then, we followed the fusion process by video-microscopy of *wt* and $hck^{-/-}$ precursors into giant cells by transducing cells with mCherry-LifeAct to stain F-actin (Supplemental Movie S1). We observed that the time course of the fusion process and the presence of podosomes that polarize at the fusion site (40) were similar in the two genotypes. In summary, Hck is not necessary for OC formation *in vitro*.

Hck is required for podosome organization and function in pre-OCs but not in mature OCs that overexpress Src

Since Hck is involved in the formation and stability of podosomes in macrophages (23, 25), we next looked at the role of Hck in the organization and function of podosomes during OC differentiation. Cells were
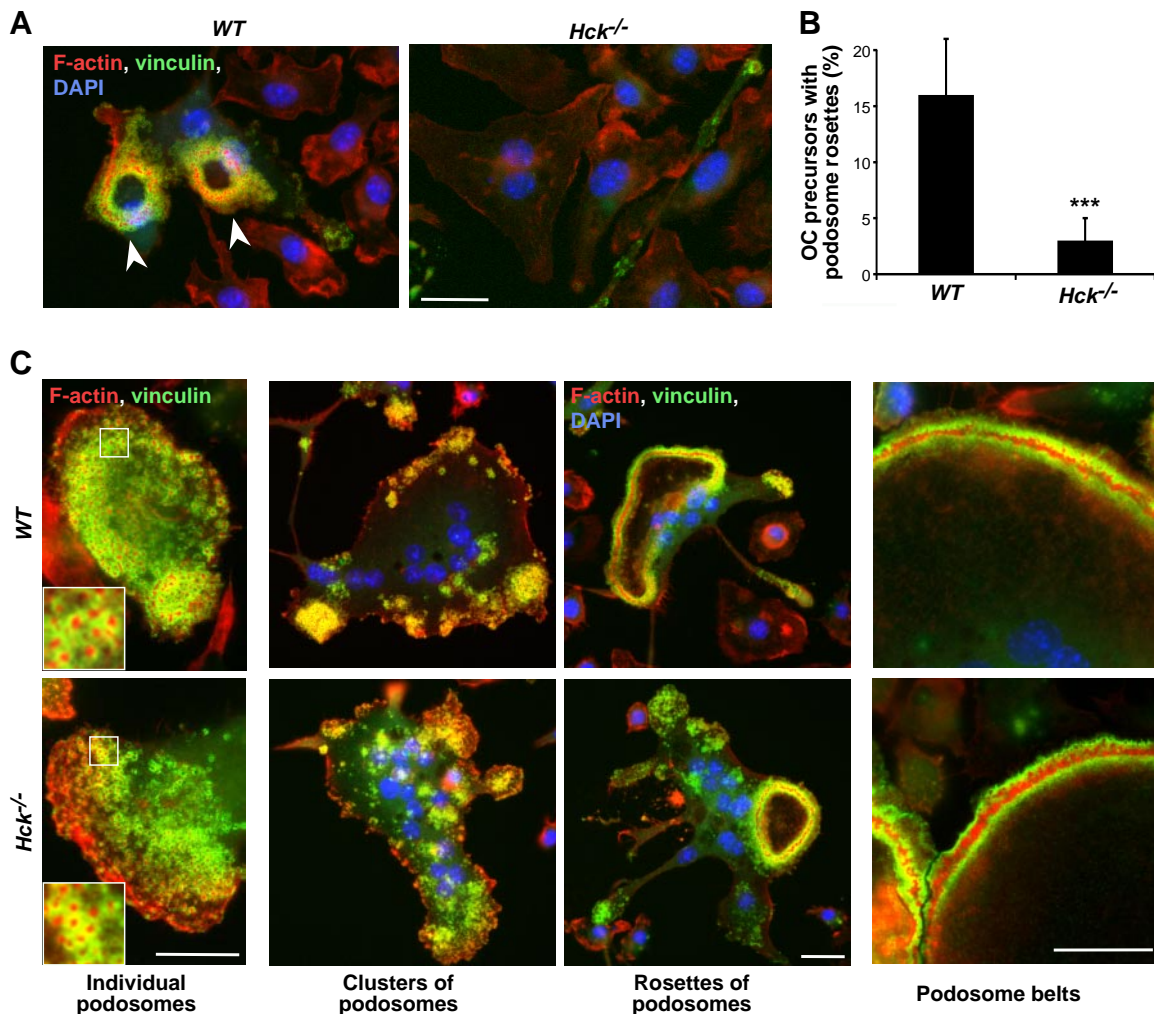

Figure 3. Podosome organization is defective in $hck^{-/-}$ pre-OCs, but normal in mature OCs. *A*) Immunofluorescence microscopy of *wt* and $hck^{-/-}$ pre-OCs. Cells were stained with antibodies against vinculin (green), Texas red-coupled phalloidin (F-actin, red) and DAPI (nuclei, blue). Merged images are shown. White arrowheads point to podosome rosettes that are mostly absent in $hck^{-/-}$ pre-OCs. Scale bar = 10 μm. *B*) Percentage of pre-OCs exhibiting podosome rosettes (means±SD of 3 independent experiments, ≥100 cells/experiment). *C*) Immunofluorescence microscopy of mature OCs from *wt* and $hck^{-/-}$ precursors. Cells were stained as in *A*. Merged images show individual podosomes (left panels) and podosomes organized as clusters or rings (middle panels) or belts (right panels), which are organized normally in $hck^{-/-}$ mature OCs. Insets: 2.7-fold magnification of boxed areas. Scale bars = 10 μm.

stained for F-actin and vinculin to visualize podosomes. Pre-OCs, defined as adherent, mononucleated, and TRAP-positive cells, were obtained at d 3 of bone marrow mononuclear cell differentiation (31). Whereas 15% of w*t* pre-OCs formed podosomes organized as rosettes, only 3% of $hck^{-/-}$ pre-OCs formed podosome rosettes (**Fig. 3A**, **B**). To explore the matrix degradation activity of podosomes in pre-OCs, gelatin-FITC degradation assay was used. *wt* pre-OCs degraded gelatin-FITC and, as expected for cells that have a defective formation of podosome rosettes (24), $hck^{-/-}$ pre-OCs had a signifi-

cantly lower capacity to degrade this matrix (Supplemental Fig. S2).

When mature OCs obtained at d 5 of differentiation were examined, no difference in podosome formation and organization was noticed (Fig. 3*C*). Microscopic observation of individual podosomes in $hck^{-/-}$ OCs revealed that they were classically organized as an F-actin core (Fig. 3*C*, red) surrounded by vinculin (Fig. 3*C*, green). Most of the cells organized their podosomes in three patterns: clusters, rings, and belts, as described previously (10). Similarly to *wt* OCs, ~30% of mature $hck^{-/-}$ OCs exhib-
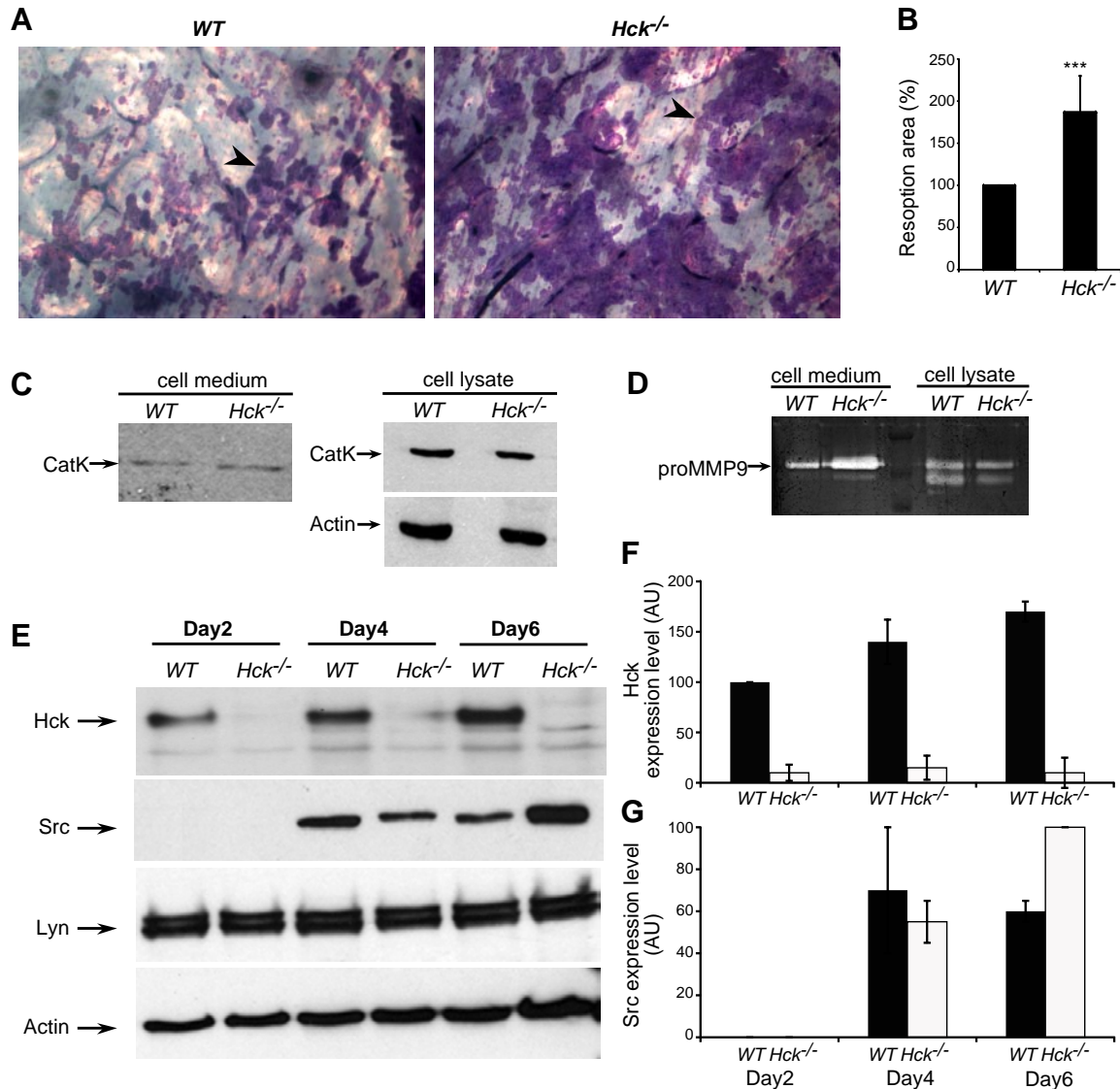
Figure 4. Bone resorption is increased and Src is overexpressed in $hck^{-/-}$ mature OCs. *A*) Bone marrow mononuclear cells from *wt* and $hck^{-/-}$ mice were seeded on bovine bone slides and differentiated into OCs with M-CSF and RANKL for 10 d. Then, OCs were lysed and bone slices were stained with toluidine blue to visualize resorption pits. Representative images of bone-resorption pits (violet, indicated by black arrowheads) generated by OCs. *B*) Quantitative data of results from *A* show an increase in bone degradation by $hck^{-/-}$ OCs. Data were obtained from 6 independent experiments. *C*) Western blot analysis of OC supernatants (cell medium, left panels) and of OC total extracts (cell lysate, right panel) was performed using antibodies directed against cathepsin K and actin (as a loading control). *D*) Gelatin zymograph of OC supernatants (cell medium, left panels) and of OC total extracts (cell lysate, right panel) show that MMP9 activity is increased in $hck^{-/-}$ mature OCs. *C* and *D* show a representative experiment out of 3 independent experiments. *E*) Western blot analysis of total cell extracts was performed using antibodies directed against Hck, Src, Lyn, and actin (as a loading control). The two isoforms of Hck migrated as a single band. *F*, *G*) Quantification of Hck (*F*) and Src (*G*) expression levels show that *Src* is overexpressed in $hck^{-/-}$ mature OC. Arbitrary units (AU) represent the signal intensity measured with Adobe Photoshop, in 3 experiments.
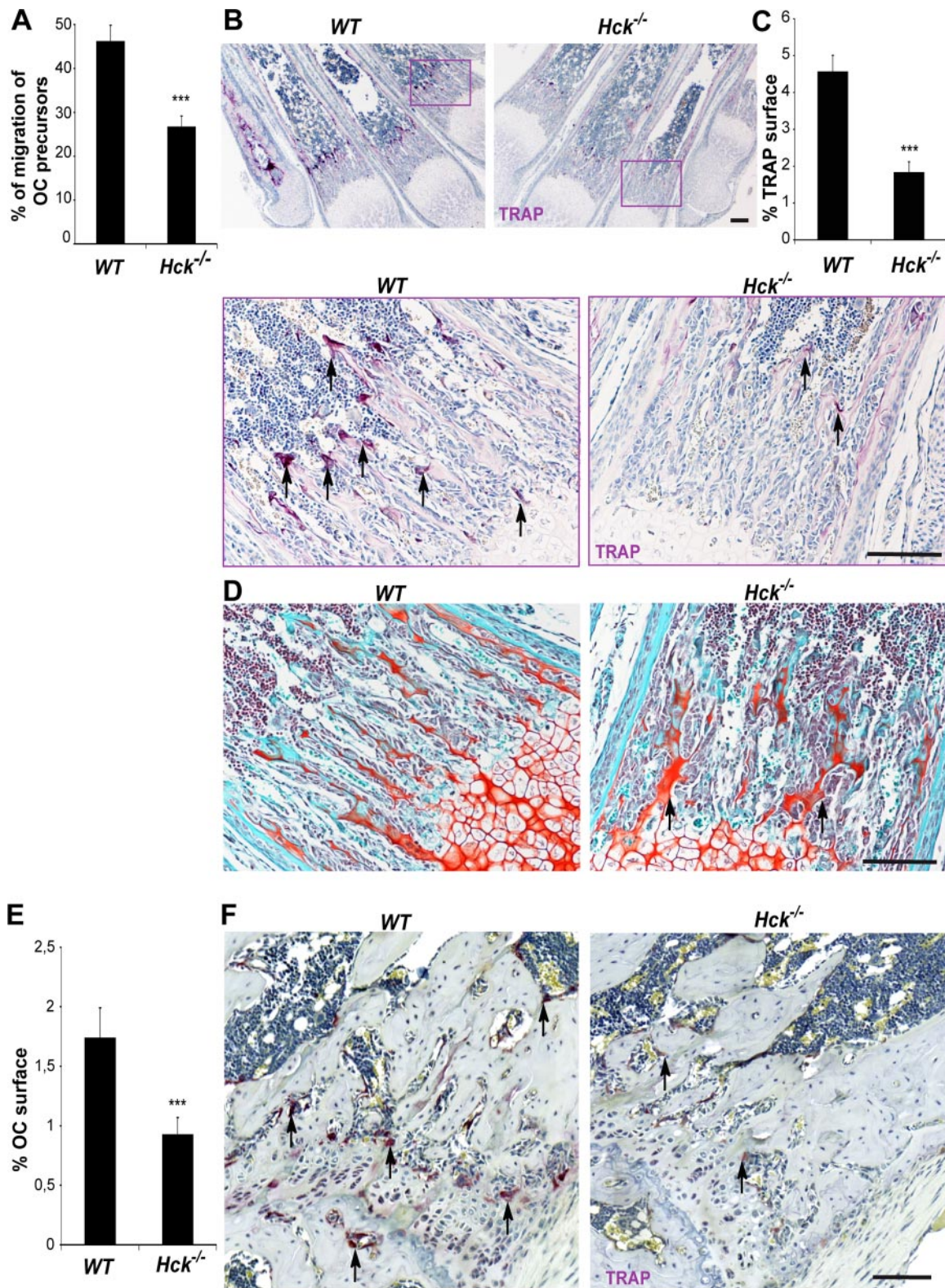
Figure 5. Migration of $hck^{-/-}$ pre-OCs is defective *in vitro* and *in vivo*. *A*) Pre-OCs (d 3 of differentiation) were seeded on thick matrices of Matrigel and allowed to migrate. The percentage of $hck^{-/-}$ pre-OCs infiltrating the matrices quantified after 48 h of migration is decreased compared to *wt* (means±SD of 3 independent experiments). *B*) Representative histological sections of metatarsals of 1-wk-old *wt* and $hck^{-/-}$ mice stained with TRAP to visualize OCs (black arrows) and counterstained with hematoxylin. Bottom panels show 6-fold magnification of boxed areas in top panels. Scale bars = 100 μm. *C*) Surface occupied by TRAP-positive signal was quantified per bone surface in 6 separate histological sections per mouse (n=5 mice/phenotype). Number of TRAP-positive cells in $hck^{-/-}$ is significantly diminished. Error bars = SEM. *D*) Staining of metatarsals with Safranine O/Fast green to visualize cartilage (red) and bone formation (blue) show a defect in trabeculae organization in 1-wk-old $hck^{-/-}$

(continued on next page)

ited podosome clusters, 20% had rings, and 50% formed belts (Fig. 3*C* and Supplemental Fig. S3). In addition, when OCs were differentiated on ostologic bone slices, the formation of sealing zones was normal in $hck^{-/-}$ OCs (not shown) compared to *wt*.

The formation of podosomes and their organization as a sealing zone, where proteolytic enzymes are released, are critical for the bone-resorption activity of mature OCs (6). To examine the bone degradation activity, we used the classical assay that consists of differentiation of OCs on bovine cortical bone slices. After 10 d, resorption pits were visualized by toluidine blue staining. In contrast to what was expected based on the *in vivo* phenotype, the size of the resorption lacunae formed by $hck^{-/-}$ OCs was significantly enhanced compared to *wt* OCs (**Fig. 4*A, B***). Similar results were obtained on dentine slices or when mature OCs were harvested from culture dishes and plated on bone slices for 48 h (data not shown).

To determine why mature $hck^{-/-}$ OCs are more efficient to resorb bone than their *wt* counterparts, we measured the level and the activity of cathepsin K and MMP9 in *wt vs.* $hck^{-/-}$ OCs, because bone resorption occurs upon secretion of these proteases within the sealing zone (41). Western blot analysis revealed that cathepsin K production and secretion were not different in mature $hck^{-/-}$ OCs compared to *wt* OCs (Fig. 4*C*). However, gelatin zymography assay showed that MMP9 enzymatic activity was significantly increased in $hck^{-/-}$ OC supernatants compared to controls (Fig. 4*D*).

Src has been involved in the formation and stability of podosomes in OCs (16) and in the regulation of MMP9 expression (42). As it has been proposed that Hck and Src could compensate each other in OCs (17), we considered the possibility that Src could compensate for Hck deletion in mature OCs. Thus, Src and Hck expression levels were analyzed along osteoclastogenesis. In *wt* cells, we noticed that the expression of Hck increased progressively and was up 1.7-fold in mature OCs compared to cells at d 2 of differentiation (Fig. 4*E, F*). When OC differentiation was carried out with human blood monocytes, a similar increase in Hck expression was observed (not shown). Interestingly, the expression of Src was almost 2-fold higher in mature $hck^{-/-}$ OCs compared to *wt* OCs (Fig. 4*E, G*). At early time points of differentiation, Src was either not detectable or expressed at the same level in *wt* and $hck^{-/-}$ cells. In contrast to Src, Lyn expression did not vary along differentiation and did not vary in $hck^{-/-}$ OCs compared to *wt* (Fig. 4*E*). Taken together, Hck deletion affects the formation of podosomes in pre-OCs, and, consequently, the matrix degradation activity is altered. In mature OCs in which Src is overexpressed, these defects are not observed, which suggests that Src could compensate for Hck deletion.

Migration of $hck^{-/-}$ pre-OCs is impaired *in vitro*, and the number of OCs is reduced in bones of $hck^{-/-}$ mice

In addition to their role in the bone resorptive activity of OCs, podosomes have been more recently involved in the protease-dependent migration in 3D environments, called the mesenchymal migration mode (24–26, 37). As $hck^{-/-}$ pre-OCs exhibit a defect in podosome organization, we examined their transmatrix migration capacity. In Matrigel, a poorly porous matrix in which macrophages migrate in 3D using the mesenchymal mode (37), pre-OCs from *wt* and $hck^{-/-}$ cultures seeded on the top of the matrix were round, whereas they harbored the characteristic elongated shape of the mesenchymal movement inside the matrix (data not shown and ref. 37). Compared to *wt*, the number of $hck^{-/-}$ pre-OCs infiltrating the matrix was reduced significantly (**Fig. 5*A***). In contrast, mature OCs from *wt* and $hck^{-/-}$ precursors showed similar 3D-migration capacities (42±10% of migrating cells for *wt* mature OCs *vs.* 45±6% for $hck^{-/-}$ OCs), which is consistent with normal podosome organization.

The migration defect observed in $hck^{-/-}$ pre-OCs was then investigated *in vivo*. To this end, we examined metatarsals from *wt* and $hck^{-/-}$ 1-wk-old mice, where endochondral ossification occurs with rapid bone growth depending on OC recruitment (43). Histological analysis showed that the number of TRAP-positive cells was reduced by more than half in $hck^{-/-}$ metatarsals compared to *wt* (Fig. 5*B, C*). Furthermore, we observed that the trabeculae were thickened and irregular in shape (Fig. 5*D*), indicating that the remodeling of trabeculae by OCs was defective.

Next, we examined whether this defective number of TRAP-positive cells was also observed in femurs and tibia of adult mice (8-wk-old mice). Whereas TRAP-expressing OCs were abundant and encountered along bone trabeculae in *wt* femoral metaphysis, only few OCs were observed in $hck^{-/-}$ femoral metaphysis sections (Fig. 5*E, F*). The quantification of OC number showed a 40% decrease in bones from Hck-deficient mice compared to controls (Fig. 5*E*). These data strongly support that Hck is involved in the migration of pre-OCs, resulting in a reduced number of OCs dedicated to trabecular bone remodeling with no compensatory process, as this defect persists in adults.

DISCUSSION

In this work, we examined for the first time the function of Hck in bone homeostasis. Using state of the art technology for bone investigation, we conclude that $hck^{-/-}$ mice have a moderate osteopetrotic phenotype characterized by a defect of trabecular bone remodel-

---

mice (black arrows). Scale bar = 100 μm. *E*) OC surface was quantified per bone surface in 3 separate histological sections of femurs and tibia of 8-wk-old *wt* and $hck^{-/-}$ mice (*n*=6 mice/phenotype). Number of OCs in $hck^{-/-}$ mice is significantly diminished. *F*) Representative histological sections of trabecular bone of femurs stained with TRAP to visualize OCs, indicated by black arrows, and counterstained with hematoxylin to visualize bone trabeculae. Scale bar = 100 μm. Error bars = SEM.

ing. This phenotype has not been observed in the original report on $hck^{-/-}$ mice because the techniques used did not allow the level of resolution that we present in the current study (11).

The urine and blood parameters characterizing bone formation and resorption *in vivo* indicated that $hck^{-/-}$ mice have decreased bone degradation and normal bone formation activities. Despite our observation that $hck^{-/-}$ OCs have more efficient bone degradation activity *in vitro* than their *wt* counterparts, we propose that the *in vivo* osteopetrotic phenotype is likely resulting from the lower number of OCs present in bones. As we show that osteoclastogenesis and OC viability of $hck^{-/-}$ precursors is not affected *in vitro*, these findings suggest that the decreased OC numbers in $hck^{-/-}$ mice is not the result of altered differentiation or life span. OC differentiation could be regulated not exactly in the same fashion *in vivo* and *in vitro*, but in several studies, both processes appear similar (44). Lyn, Fyn, and Src have been shown to regulate osteoclastogenesis (40, 44–47). Whereas Hck is necessary for macrophage fusion in other contexts, such as HIV-1-induced giant macrophage formation (33), we show here that Hck is not involved in the process of cell fusion along osteoclastogenesis.

As described previously in $hck^{-/-}$ macrophages (24, 25), $hck^{-/-}$ pre-OCs have a strong defect in podosome formation and organization as rosettes. The consequence is reduced proteolytic activity of the extracellular matrix and defective mesenchymal migration. These results were expected, since podosomes, and more particularly podosome rosettes, have been implicated in the protease-dependent mesenchymal migration of macrophages (24–26). Interestingly, $hck^{-/-}$ mature OCs, in which podosome organization is restored, recover the ability to migrate in 3D environments and to degrade the bone matrix. Our current findings in metatarsals of 1-wk-old mice, in which there is a strong dependency on pre-OC recruitment for bone remodeling, strongly support the idea of impaired pre-OC migration in Hck-deficient mice. Interestingly, a reduced number of TRAP-positive cells is also observed in bones of adult mice, providing a good explanation for the generalized osteopetrosis observed and indicating that the defect persists through the lifetime of the mice. To our knowledge, MMPs, and, more precisely MMP9, are the only effectors of OC recruitment to bones described to date (41, 48, 49). In $MMP9^{-/-}$ mice, defective endochondral ossification has been observed and described to delayed bone recruitment of pre-OCs (49). Thus, collectively we propose that, by regulating the formation and organization of podosome rosettes in pre-OCs, Hck controls their bone recruitment and thereby controls the number of mature OCs in bones. It has been recently established that osteoclast precursors are recruited from the blood circulation to bones (5), and thus they are expected to cross several anatomical barriers. Our results provide a new contribution to understanding the mechanisms involved in OC recruitment by identifying Hck as an effector of the migration of pre-OCs to bones.

In mature $hck^{-/-}$ OCs, podosome formation, organization and bone degradative activity are normal. A compensatory mechanism of altered expression of other Src kinases could take place, as often described in other studies using mice deleted of an Src family member (17, 28, 50). We suspected that Src could compensate for Hck deletion for the following reasons: Src has been described as a regulator of several podosome parameters in OCs (16, 21), Hck expression is doubled in $src^{-/-}$ mice (17), and $src^{-/-}$ $hck^{-/-}$ mice have more severe osteopetrosis than the single-mutant mice (17). Supporting our hypothesis, we observed that Src is 1.7-fold overexpressed in mature $hck^{-/-}$ OCs in comparison with *wt* cells, while Lyn expression was not modified. Interestingly, Src overexpression occurred at the late stage of OC differentiation. Thus, if we assume that Src overexpression is compensating for Hck deletion, the phenotype of pre-OCs, in which Src is not overexpressed, is clearly the only situation in which Hck function alone is revealed. In $src^{-/-}$ OCs, Hck is overexpressed, and both individual podosomes and podosomes organized as clusters are formed. Therefore, we propose that Hck is involved in podosome formation and organization but not in the formation of podosome belts or sealing zones, which are more likely a specific function of Src in mature OCs. An intriguing observation in $src^{-/-}$ mice is the number of OCs in bones that is doubled. Now we can explain it by proposing that Hck overexpression in $src^{-/-}$ mice (17) might favor pre-OC migration and thereby partially compensate for the bone-resorption defect of mature OCs. The $src^{-/-}$ phenotype has been classified as a rich osteoclast osteopetrosis (for an extensive review, see ref. 51), contrary to Hck, which we describe as a poor osteoclast osteopetrosis. The specificity of the two phenotypes can explain why in $src^{-/-}$ $hck^{-/-}$ double-knockout mice the osteopetrotic phenotype is more severe than in the simple-knockout $src^{-/-}$. In addition, the following two observations are also in favor of a less important defect in bone homeostasis for $hck^{-/-}$ mice than $src^{-/-}$ mice. First, $hck^{-/-}$ OCs release more MMP9 than *wt* OCs. MMP9 expression has been shown to be enhanced by Src activation in tumor cells (42). Thus, in addition to restoration of a normal podosome organization, we propose that Src overexpression in $hck^{-/-}$ OCs could also participate in the increased bone-resorption activity of $hck^{-/-}$ OCs through MMP9 overexpression. This highly degrading function of $hck^{-/-}$ OCs, however, does not compensate for their reduced number in bones and does not abolish the osteopetrotic phenotype. Second, the differentiation and bone formation activity of osteoblasts, a cell type that does not express Hck (39), have been shown to be enhanced when the expression of Src is decreased (52), thereby contributing to the much stronger osteopetrotic phenotype in $src^{-/-}$ compared to $hck^{-/-}$ mice.

In $hck^{-/-}$ mice, the osteopetrotic phenotype is characterized by a defective organization of trabeculae associated with a markedly reduced number of TRAP-positive cells in bones of newborn and adult animals. A subset of osteopetrotic phenotypes coupled with a low number or absence of OCs has been linked with weak to severe chondrodysplasia (53–55). Intriguingly, we did not observe any defect in the growth plate of young $hck^{-/-}$ mice. Normal vascularization and degradation

of hypertrophic cartilage seems to occur, indicating that hck deficiency does not impede the action of septoclasts (56, 57) and chondroclasts (58), the main TRAP-positive cell types implicated in chondrodysplasia. Thus, it is likely that the role of Hck in bone could be restricted to a subpopulation of pre-OCs (59).

In summary, this study provides insight into the interplay between members of the Src family, clearly showing both independent and redundant roles. We show for the first time the role of Hck in OC and bone homeostasis, including a function not shared with Src, the recruitment of pre-OCs to bones. In pre-OCs, Hck plays a critical role in the organization of podosomes and cell migration, which likewise explains the diminished number of TRAP-positive cells in bones of $hck^{-/-}$ mice and the osteopetrotic phenotype. Recent studies have shown that OCs are involved in the pathogenesis of bone and joint destruction in rheumatoid arthritis (60). Pharmacological inhibitors of Hck and Src may decrease OC recruitment and bone degradation activity and may be used as novel treatments for rheumatoid arthritis. FJ

REFERENCES

1. Boyle, W. J., Simonet, W. S., and Lacey, D. L. (2003) Osteoclast differentiation and activation. *Nature* **423**, 337–342
2. Gallois, A., Mazzorana, M., Vacher, J., and Jurdic, P. (2009) Osteoimmunology: an integrated vision of immune and bone systems. *Med. Sci. (Paris)* **25**, 259–265
3. Vignery, A. (2008) Macrophage fusion: molecular mechanisms. *Methods Mol. Biol.* **475**, 149–161
4. Andersen, T. L., Sondergaard, T. E., Skorzynska, K. E., Dagnaes-Hansen, F., Plesner, T. L., Hauge, E. M., Plesner, T., and Delaisse, J. M. (2009) A physical mechanism for coupling bone resorption and formation in adult human bone. *Am. J. Pathol.* **174**, 239–247
5. Kotani, M., Kikuta, J., Klauschen, F., Chino, T., Kobayashi, Y., Yasuda, H., Tamai, K., Miyawaki, A., Kanagawa, O., Tomura, M., and Ishii, M. (2013) Systemic circulation and bone recruitment of osteoclast precursors tracked by using fluorescent imaging techniques. *J. Immunol.* **190**, 605–612
6. Jurdic, P., Saltel, F., Chabadel, A., and Destaing, O. (2006) Podosome and sealing zone: specificity of the osteoclast model. *Eur. J. Cell Biol.* **85**, 195–202
7. Teitelbaum, S. L. (2011) The osteoclast and its unique cytoskeleton. *Ann. N. Y. Acad. Sci.* **1240**, 14–17
8. Luxenburg, C., Addadi, L., and Geiger, B. (2006) The molecular dynamics of osteoclast adhesions. *Eur. J. Cell Biol.* **85**, 203–211
9. Linder, S. (2007) The matrix corroded: podosomes and invadopodia in extracellular matrix degradation. *Trends Cell Biol.* **17**, 107–117
10. Destaing, O., Saltel, F., Geminard, J. C., Jurdic, P., and Bard, F. (2003) Podosomes display actin turnover and dynamic self-organization in osteoclasts expressing actin-green fluorescent protein. *Mol. Biol. Cell* **14**, 407–416
11. Soriano, P., Montgomery, C., Geske, R., and Bradley, A. (1991) Targeted disruption of the c-src proto-oncogene leads to osteopetrosis in mice. *Cell* **64**, 693–702
12. Horne, W. C., Sanjay, A., Bruzzaniti, A., and Baron, R. (2005) The role(s) of Src kinase and Cbl proteins in the regulation of osteoclast differentiation and function. *Immunol. Rev.* **208**, 106–125
13. Boyce, B. F., Yoneda, T., Lowe, C., Soriano, P., and Mundy, G. R. (1992) Requirement of pp60c-src expression for osteoclasts to form ruffled borders and resorb bone in mice. *J. Clin. Invest.* **90**, 1622–1627
14. Lowe, C., Yoneda, T., Boyce, B. F., Chen, H., Mundy, G. R., and Soriano, P. (1993) Osteopetrosis in Src-deficient mice is due to an autonomous defect of osteoclasts. *Proc. Natl. Acad. Sci. U. S. A.* **90**, 4485–4489
15. Schwartzberg, P. L., Xing, L., Hoffmann, O., Lowell, C. A., Garrett, L., Boyce, B. F., and Varmus, H. E. (1997) Rescue of osteoclast function by transgenic expression of kinase-deficient Src in $src^{-/-}$ mutant mice. *Genes Dev.* **11**, 2835–2844
16. Destaing, O., Sanjay, A., Itzstein, C., Horne, W. C., Toomre, D., De Camilli, P., and Baron, R. (2008) The tyrosine kinase activity of c-Src regulates actin dynamics and organization of podosomes in osteoclasts. *Mol. Biol. Cell* **19**, 394–404
17. Lowell, C. A., Niwa, M., Soriano, P., and Varmus, H. E. (1996) Deficiency of the Hck and Src tyrosine kinases results in extreme levels of extramedullary hematopoiesis. *Blood* **87**, 1780–1792
18. Miyazaki, T., Tanaka, S., Sanjay, A., and Baron, R. (2006) The role of c-Src kinase in the regulation of osteoclast function. *Mod. Rheumatol.* **16**, 68–74
19. Quintrell, N., Lebo, R., Varmus, H., Bishop, J. M., Pettenati, M. J., Le Beau, M. M., Diaz, M. O., and Rowley, J. D. (1987) Identification of a human gene (HCK) that encodes a protein-tyrosine kinase and is expressed in hemopoietic cells. *Mol. Cell. Biol.* **7**, 2267–2275
20. Ziegler, S. F., Marth, J. D., Lewis, D. B., and Perlmutter, R. M. (1987) Novel protein-tyrosine kinase gene (Hck) preferentially expressed in cells of hematopoietic origin. *Mol. Cell. Biol.* **7**, 2276–2285
21. Luxenburg, C., Parsons, J. T., Addadi, L., and Geiger, B. (2006) Involvement of the Src-cortactin pathway in podosome formation and turnover during polarization of cultured osteoclasts. *J. Cell Sci.* **119**, 4878–4888
22. Poincloux, R., Vincent, C., Labrousse, A., Castandet, J., Rigo, M., Cougoule, C., Bordier, C., Le Cabec, V., and Maridonneau-Parini, I. (2006) Re-arrangements of podosome structures are observed when Hck is activated in myeloid cells. *Eur. J. Cell Biol.* **85**, 327–332
23. Cougoule, C., Carreno, S., Castandet, J., Labrousse, A., Astarie-Dequeker, C., Poincloux, R., Le Cabec, V., and Maridonneau-Parini, I. (2005) Activation of the lysosome-associated p61Hck isoform triggers the biogenesis of podosomes. *Traffic* **6**, 682–694
24. Cougoule, C., Le Cabec, V., Poincloux, R., Al Saati, T., Mege, J. L., Tabouret, G., Lowell, C. A., Laviolette-Malirat, N., and Maridonneau-Parini, I. (2010) Three-dimensional migration of macrophages requires Hck for podosome organization and extracellular matrix proteolysis. *Blood* **115**, 1444–1452
25. Guiet, R., Verollet, C., Lamsoul, I., Cougoule, C., Poincloux, R., Labrousse, A., Calderwood, D. A., Glogauer, M., Lutz, P. G., and Maridonneau-Parini, I. (2012) Macrophage mesenchymal migration requires podosome stabilization by filamin A. *J. Biol. Chem.* **287**, 13051–13062
26. Cougoule, C., Van Goethem, E., Le Cabec, V., Lafouresse, F., Dupre, L., Mehraj, V., Mege, J. L., Lastrucci, C., and Maridonneau-Parini, I. (2012) Blood leukocytes and macrophages of various phenotypes have distinct abilities to form podosomes and to migrate in 3D environments. *Eur. J. Cell Biol.* **91**, 938–949
27. Verollet, C., Charriere, G. M., Labrousse, A., Cougoule, C., Le Cabec, V., and Maridonneau-Parini, I. (2011) Extracellular proteolysis in macrophage migration: losing grip for a breakthrough. *Eur. J. Immunol.* **41**, 2805–2813

28. Lowell, C. A., Soriano, P., and Varmus, H. E. (1994) Functional overlap in the src gene family: inactivation of hck and fgr impairs natural immunity. *Genes Dev.* **8,** 387–398

29. Mugniery, E., Dacquin, R., Marty, C., Benoist-Lasselin, C., de Vernejoul, M. C., Jurdic, P., Munnich, A., Geoffroy, V., and Legeai-Mallet, L. (2012) An activating Fgfr3 mutation affects trabecular bone formation via a paracrine mechanism during growth. *Human Mol. Genet.* **21,** 2503–2513

30. Ortega, N., Behonick, D. J., Colnot, C., Cooper, D. N., and Werb, Z. (2005) Galectin-3 is a downstream regulator of matrix metalloproteinase-9 function during endochondral bone formation. *Mol. Biol. Cell* **16,** 3028–3039

31. Dacquin, R., Domenget, C., Kumanogoh, A., Kikutani, H., Jurdic, P., and Machuca-Gayet, I. (2011) Control of bone resorption by semaphorin 4D is dependent on ovarian function. *PLoS ONE* **6,** e26627

32. Carreno, S., Caron, E., Cougoule, C., Emorine, L. J., and Maridonneau-Parini, I. (2002) p59Hck isoform induces F-actin reorganization to form protrusions of the plasma membrane in a Cdc42- and Rac-dependent manner. *J. Biol. Chem.* **277,** 21007–21016

33. Verollet, C., Zhang, Y. M., Le Cabec, V., Mazzolini, J., Charriere, G., Labrousse, A., Bouchet, J., Medina, I., Biessen, E., Niedergang, F., Benichou, S., and Maridonneau-Parini, I. (2010) HIV-1 Nef triggers macrophage fusion in a p61Hck- and protease-dependent manner. *J. Immunol.* **184,** 7030–7039

34. Pandruvada, S. N., Yuvaraj, S., Liu, X., Sundaram, K., Shanmugarajan, S., Ries, W. L., Norris, J. S., London, S. D., and Reddy, S. V. (2010) Role of CXC chemokine ligand 13 in oral squamous cell carcinoma associated osteolysis in athymic mice. *Int. J. Cancer* **126,** 2319–2329

35. Harre, U., Georgess, D., Bang, H., Bozec, A., Axmann, R., Ossipova, E., Jakobsson, P. J., Baum, W., Nimmerjahn, F., Szarka, E., Sarmay, G., Krumbholz, G., Neumann, E., Toes, R., Scherer, H. U., Catrina, A. I., Klareskog, L., Jurdic, P., and Schett, G. (2012) Induction of osteoclastogenesis and bone loss by human autoantibodies against citrullinated vimentin. *J. Clin. Invest.* **122,** 1791–1802

36. Villeneuve, C., Gilleron, M., Maridonneau-Parini, I., Daffe, M., Astarie-Dequeker, C., and Etienne, G. (2005) Mycobacteria use their surface-exposed glycolipids to infect human macrophages through a receptor-dependent process. *J. Lipid Res.* **46,** 475–483

37. Van Goethem, E., Poincloux, R., Gauffre, F., Maridonneau-Parini, I., and Le Cabec, V. (2010) Matrix architecture dictates three-dimensional migration modes of human macrophages: differential involvement of proteases and podosome-like structures. *J. Immunol.* **184,** 1049–1061

38. Labernadie, A., Thibault, C., Vieu, C., Maridonneau-Parini, I., and Charriere, G. M. (2010) Dynamics of podosome stiffness revealed by atomic force microscopy. *Proc. Natl. Acad. Sci. U. S. A.* **107,** 21016–21021

39. Daino, K., Ugolin, N., Altmeyer-Morel, S., Guilly, M. N., and Chevillard, S. (2009) Gene expression profiling of alpha-radiation-induced rat osteosarcomas: identification of dysregulated genes involved in radiation-induced tumorigenesis of bone. *Int. J. Cancer* **125,** 612–620

40. Oikawa, T., Oyama, M., Kozuka-Hata, H., Uehara, S., Udagawa, N., Saya, H., and Matsuo, K. (2012) Tks5-dependent formation of circumferential podosomes/invadopodia mediates cell-cell fusion. *J. Cell Biol.* **197,** 553–568

41. Ortega, N., Behonick, D., Stickens, D., and Werb, Z. (2003) How proteases regulate bone morphogenesis. *Ann. N. Y. Acad. Sci.* **995,** 109–116

42. Luo, Y., Liang, F., and Zhang, Z. Y. (2009) PRL1 promotes cell migration and invasion by increasing MMP2 and MMP9 expression through Src and ERK1/2 pathways. *Biochemistry* **48,** 1838–1846

43. Wagner, E. F., and Karsenty, G. (2001) Genetic control of skeletal development. *Curr. Opin. Genet. Dev.* **11,** 527–532

44. Kim, H. J., Zhang, K., Zhang, L., Ross, F. P., Teitelbaum, S. L., and Faccio, R. (2009) The Src family kinase, Lyn, suppresses osteoclastogenesis in vitro and in vivo. *Proc. Natl. Acad. Sci. U. S. A.* **106,** 2325–2330

45. Winograd-Katz, S. E., Brunner, M. C., Mirlas, N., and Geiger, B. (2011) Analysis of the signaling pathways regulating Src-dependent remodeling of the actin cytoskeleton. *Eur. J. Cell Biol.* **90,** 143–156

46. Kim, H. J., Warren, J. T., Kim, S. Y., Chappel, J. C., DeSelm, C. J., Ross, F. P., Zou, W., and Teitelbaum, S. L. (2010) Fyn promotes proliferation, differentiation, survival and function of osteoclast lineage cells. *J. Cell. Biochem.* **111,** 1107–1113

47. Kim, H. S., Kim, D. K., Kim, A. R., Mun, S. H., Lee, S. K., Kim, J. H., Kim, Y. M., and Choi, W. S. (2012) Fyn positively regulates the activation of DAP12 and FcRgamma-mediated costimulatory signals by RANKL during osteoclastogenesis. *Cell. Signal.* **24,** 1306–1314

48. Blavier, L., and Delaisse, J. M. (1995) Matrix metalloproteinases are obligatory for the migration of preosteoclasts to the developing marrow cavity of primitive long bones. *J. Cell Sci.* **108**(Pt. 12), 3649–3659

49. Engsig, M. T., Chen, Q. J., Vu, T. H., Pedersen, A. C., Therkidsen, B., Lund, L. R., Henriksen, K., Lenhard, T., Foged, N. T., Werb, Z., and Delaisse, J. M. (2000) Matrix metalloproteinase 9 and vascular endothelial growth factor are essential for osteoclast recruitment into developing long bones. *J. Cell Biol.* **151,** 879–889

50. Guiet, R., Poincloux, R., Castandet, J., Marois, L., Labrousse, A., Le Cabec, V., and Maridonneau-Parini, I. (2008) Hematopoietic cell kinase (Hck) isoforms and phagocyte duties—from signaling and actin reorganization to migration and phagocytosis. *Eur. J. Cell Biol.* **87,** 527–542

51. Henriksen, K., Bollerslev, J., Everts, V., and Karsdal, M. A. (2011) Osteoclast activity and subtypes as a function of physiology and pathology–implications for future treatments of osteoporosis. *Endocrine Rev.* **32,** 31–63

52. Marzia, M., Sims, N. A., Voit, S., Migliaccio, S., Taranta, A., Bernardini, S., Faraggiana, T., Yoneda, T., Mundy, G. R., Boyce, B. F., Baron, R., and Teti, A. (2000) Decreased c-Src expression enhances osteoblast differentiation and bone formation. *J. Cell Biol.* **151,** 311–320

53. Kim, N., Odgren, P. R., Kim, D. K., Marks, S. C., Jr., and Choi, Y. (2000) Diverse roles of the tumor necrosis factor family member TRANCE in skeletal physiology revealed by TRANCE deficiency and partial rescue by a lymphocyte-expressed TRANCE transgene. *Proc. Natl. Acad. Sci. U. S. A.* **97,** 10905–10910

54. Ortega, N., Wang, K., Ferrara, N., Werb, Z., and Vu, T. H. (2010) Complementary interplay between matrix metalloproteinase-9, vascular endothelial growth factor and osteoclast function drives endochondral bone formation. *Disease Models Mech.* **3,** 224–235

55. Vu, T. H., Shipley, J. M., Bergers, G., Berger, J. E., Helms, J. A., Hanahan, D., Shapiro, S. D., Senior, R. M., and Werb, Z. (1998) MMP-9/gelatinase B is a key regulator of growth plate angiogenesis and apoptosis of hypertrophic chondrocytes. *Cell* **93,** 411–422

56. Gartland, A., Mason-Savas, A., Yang, M., MacKay, C. A., Birnbaum, M. J., and Odgren, P. R. (2009) Septoclast deficiency accompanies postnatal growth plate chondrodysplasia in the toothless (tl) osteopetrotic, colony-stimulating factor-1 (CSF-1)-deficient rat and is partially responsive to CSF-1 injections. *Am. J. Pathol.* **175,** 2668–2675

57. Lee, E. R., Lamplugh, L., Shepard, N. L., and Mort, J. S. (1995) The septoclast, a cathepsin B-rich cell involved in the resorption of growth plate cartilage. *J. Histochem. Cytochem.* **43,** 525–536

58. Gerber, H. P., Vu, T. H., Ryan, A. M., Kowalski, J., Werb, Z., and Ferrara, N. (1999) VEGF couples hypertrophic cartilage remodeling, ossification and angiogenesis during endochondral bone formation. *Nat. Med.* **5,** 623–628

59. Everts, V., de Vries, T. J., and Helfrich, M. H. (2009) Osteoclast heterogeneity: lessons from osteopetrosis and inflammatory conditions. *Biochim. Biophys. Acta* **1792,** 757–765

60. Byeon, S. E., Yi, Y. S., Oh, J., Yoo, B. C., Hong, S., and Cho, J. Y. (2012) The role of Src kinase in macrophage-mediated inflammatory responses. *Mediators Inflamm.* **2012,** 512926